Pulsed-beam propagation in lossless dispersive media. II. A numerical example

Timor Melamed and Leopold B. Felsen*

Department of Aerospace and Mechanical Engineering, Boston University, 110 Cummington Street, Boston, Massachusetts 02215

Received September 2, 1997; accepted December 2, 1997; revised manuscript received January 15, 1998

In Part I of this two-part investigation we presented a theory for propagation of pulsed-beam wave packets in a homogeneous lossless dispersive medium with the generic dispersion relation $k(\omega)$. Emphasis was placed on the paraxial regime, and detailed studies were performed to parameterize the effect of dispersion in terms of specific physical footprints associated with the PB field and with properties of the $k(\omega)$ dispersion surface. Moreover, critical nondimensional combinations of these footprints were defined to ascertain the space–time range of applicability of the paraxial approximation. This was done by recourse to simple saddle-point asymptotics in the Fourier inversion integral from the frequency domain, with restrictions to the fully dispersive regime sufficiently far behind the wave front. Here we extend these studies by addressing the dispersive-to-nondispersive transition as the observer moves toward the wave front. It is now necessary to adopt a model for the dispersive properties to correct the nondispersive high-frequency limit $k(\omega) = \omega/c$ with higher-order terms in $(1/\omega)$. A simple Lorentz model has been chosen for this purpose that allows construction of a simple uniform transition function which connects smoothly onto the near-wave-front-reduced generic $k(\omega)$ profile. This model is also used for assessing the accuracy of the various analytic parameterizations and estimates in part I through comparison with numerically generated reference solutions. It is found that both the asymptotics for the pulsed-beam field and the nondimensional estimators perform remarkably well, thereby lending confidence to the notion that the critical parameter combinations are well matched to the space–time wave dynamics. © 1998 Optical Society of America [S0740-3232(98)02505-8]

OCIS codes: 260.2030, 050.1940, 270.5530, 350.5500.

1. INTRODUCTION

This paper is concerned with extending the investigation of paraxial pulsed-beam (PB) wave-packet propagation in homogeneous lossless dispersive media performed in Part I,[1] and with validating the analytic space–time results given in Part I by application to a specific example. In Part I the medium was characterized by a generic dispersion relation $k(\omega)$, and the emphasis was placed on the fully developed dispersive regime. Various critical nondimensional parameters were identified that expressed the effects of dispersion in terms of physical footprints pertaining to the PB wave objects as well as to the characteristics of the dispersion surface. To extend the results of Part I from the fully dispersive regime through the weakly dispersive and eventually nondispersive regime as the observer approaches the wave front, a simple Lorentz-type dispersion model, characteristic of a cold electron plasma, has been adopted. This model allows explicit closed-form construction of a uniform field transition function that patches onto the upper frequency limit of the fully dispersive profile and reduces to the nondispersive PB as $k(\omega) \to \omega/c$ at the wave front. The cold plasma model is also used for numerical evaluation of the asymptotic solutions and estimations and for assessing their performance by comparison with direct numerical evaluation of the frequency inversion integral.

In Section 2 the cold plasma dispersion relation is defined, and all relevant asymptotic expressions for observables and estimations derived generically in Part I are reproduced here for the cold plasma case. In each case numerical calculations are implemented to quantify and calibrate the performances of the theory (see Figs. 1–5 below). References to equations, figures, section headings, etc., in Part I are identified with the prefix I [for example, relation (17) of Part I is referenced as relation (I.17)]. Section 3 is concerned with the transitional nondispersive-to-dispersive regime near the wave front. The numerical comparisons are shown in Fig. 6 below. Concluding remarks are made in Section 4.

2. PARAMETERIZATION OF THE COLD PLASMA DISPERSION FIELD

A. Time-Domain Asymptotics

To test the performance of the various asymptotic parametric estimates developed for the PB wave-packet dispersion, we consider the simple example of a cold electron plasma that has the Lorentz-type dispersion relation

$$k(\omega) = \frac{1}{c} \sqrt{\omega^2 - {\omega_0}^2}, \tag{1}$$

where ω_0 is the plasma frequency. We obtain the stationary frequency of the PB exactly by inserting Eq. (1) into Eq. (I.25). The result is

$$\omega_s = \omega_0 \Bigg/ \sqrt{1 - \left(\frac{S}{ct}\right)^2}, \tag{2}$$

so that

$$k(\omega_s) = \frac{\omega_0 S}{c^2 t} \frac{1}{\sqrt{1 - \left(\frac{S}{ct}\right)^2}},$$

$$k''(\omega_s) = \frac{-1}{c\omega_0}\left[\left(\frac{ct}{S}\right)^2 - 1\right]^{3/2}. \tag{3}$$

From Eq. (2), the on-axis stationary frequency $\omega_s(\rho = 0)$ is

$$\bar{\omega}_s = \omega_0 \bar{\Omega}/\sqrt{\bar{\Omega}^2 - 1}, \qquad \bar{\Omega} = \frac{ct}{z}. \tag{4}$$

Accordingly,

$$k(\bar{\omega}_s) = \frac{\omega_0}{c} \Big/ \sqrt{\bar{\Omega}^2 - 1}, \qquad k''(\bar{\omega}_s) = \frac{-1}{c\omega_0}(\bar{\Omega}^2 - 1)^{3/2}. \tag{5}$$

Using a second-order Taylor-series approximation for ω_s in Eq. (2), we obtain

$$\Delta_{\omega_s}(z, \rho, t) \equiv \omega_s(z, \rho, t) - \bar{\omega}_s(z, t)$$
$$= \frac{\omega_0 z \rho^2}{2c^2 t^2 (z - i\beta)} \frac{1}{\sqrt{1 - \left(\frac{z}{ct}\right)^2}^{\,3}} + O(\rho^4). \tag{6}$$

Using Eqs. (5) in Eq. (6), we obtain

$$\Delta_{\omega_s}(z, \rho, t) = -\frac{1}{2}\rho^2 \frac{1}{z - i\beta} \frac{t}{k''(\bar{\omega}_s) z^2} + O(\rho^4). \tag{7}$$

By separating $1/(z - i\beta)$ into real and imaginary parts, we find that Eq. (7) is exactly the same as Eq. (I.38) [up to $O(\rho^4)$].

The asymptotic expression of the field in Eqs. (I.18) is given by relation (I.33). For the dispersion model in Eq. (1), we may use the exact stationary frequency ω_s in Eq. (2), evaluating

$$\Psi(\mathbf{r}, t) = \Phi(\omega_s) = \omega_s t - k(\omega_s) S(\mathbf{r}),$$
$$A(\mathbf{r}, t) = \frac{-i\beta}{z - i\beta}\left[\frac{-2}{\pi i k''(\omega_s) S}\right]^{1/2}. \tag{8}$$

Using Eqs. (2) and (3), we obtain

$$\Psi(\mathbf{r}, t) = \omega_0 t \sqrt{1 - \left(\frac{S}{ct}\right)^2}. \tag{9}$$

By expanding Ψ in Eqs. (8) in a Taylor series up to fourth order and using Eqs. (I.13), (4), and (5), we obtain

$$\Psi - \Psi(\rho = 0) \equiv \Delta_\Psi$$
$$= \frac{1}{2}\rho^2 \frac{1}{z(z - i\beta)}\left[\frac{1}{4}\rho^2 \frac{1}{z - i\beta} \frac{t^2}{k''(\bar{\omega}_s) z^2} - k(\bar{\omega}_s) z\right] + O(\rho^6). \tag{10}$$

Comparing this result with the approximate phase in Eq. (I.43), one finds that the results are exactly the same up to the sixth-order term. The amplitude in Eqs. (8) differs from the approximate form in Eq. (I.35) only in that k'' is evaluated at ω_s rather than at $\bar{\omega}_s$; thus both results have the same zero-order ρ term.

The off-axis field evaluated via the asymptotic solution in Eqs. (I.57) with Eqs. (4) and (5) is compared with the reference solution obtained by fast-Fourier-transform evaluation of Eqs. (I.18) for values of $\rho/c = 0$, 0.1, 0.2 in Fig. 1. This figure clearly demonstrates the accuracy of the asymptotic result with the approximated paraxial

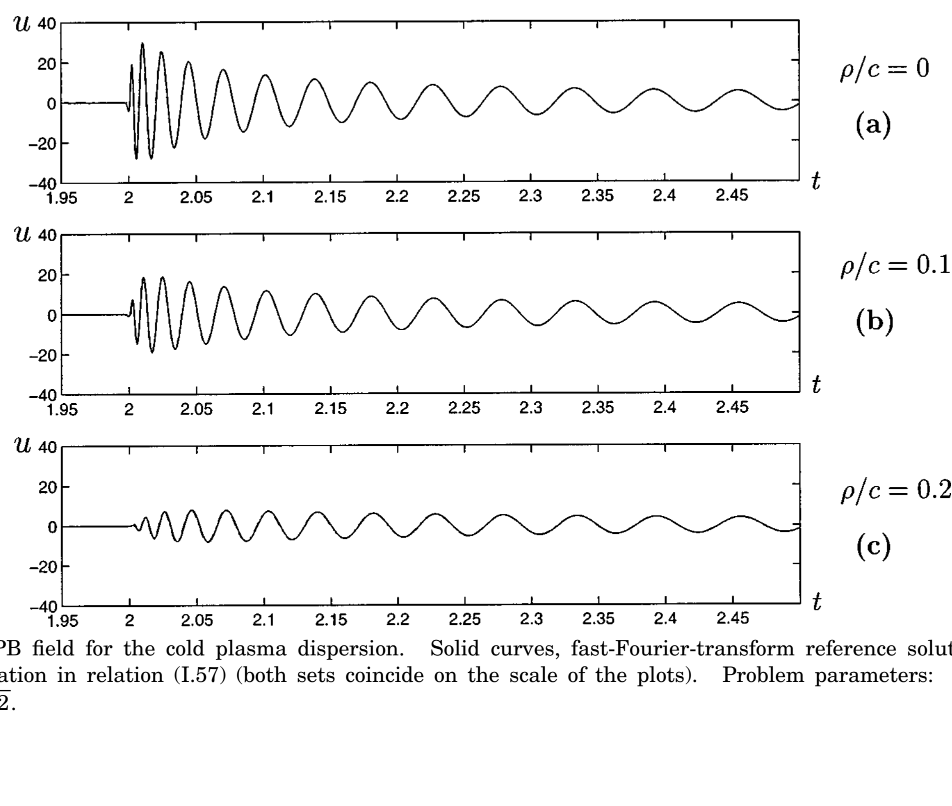

Fig. 1. Off-axis PB field for the cold plasma dispersion. Solid curves, fast-Fourier-transform reference solution; dashed curves, paraxial approximation in relation (I.57) (both sets coincide on the scale of the plots). Problem parameters: $z/c = 2$, $T = 0.005$, $\beta/c = 5$, $\omega_0 = 40\sqrt{2}$.

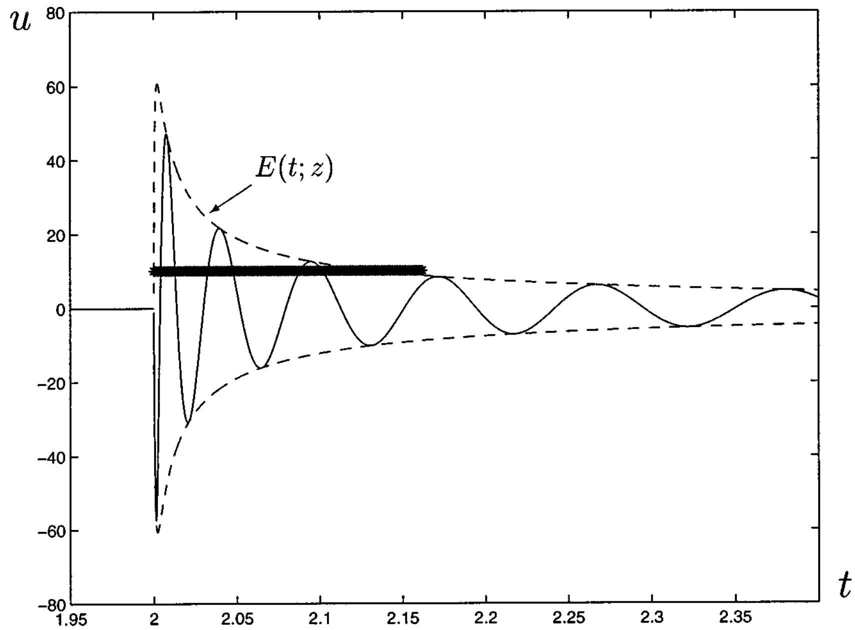

Fig. 2. Envelope function $E(t, z)$ (dashed curve) with constant z for the cold plasma dispersion. The thick line describes the approximated temporal width at $1/Q_d = 1/5.4$ of the envelope maximum. The horizontal axis is in units of time, and all other parameters bear the same normalization.

phase in Eqs. (I.57); both solutions coincide in these plots. The problem parameters are $z/c = 2$, $T = 0.005$, $\beta/c = 5$, and $\omega_0 = 40\sqrt{2}$.

B. Parameterizations via the Envelope Function

The envelope function in relation (I.61) for the PB field may be evaluated in the plasma medium by use of Eqs. (4) and (5):

$$E(z, t) = \frac{|\beta|}{|z - i\beta|}\left(\frac{2c\omega_0}{\pi z}\right)^{1/2} \times \exp(-\omega_0 T\bar{\Omega}/2\sqrt{\bar{\Omega}^2 - 1})/(\bar{\Omega}^2 - 1)^{3/4}. \tag{11}$$

The envelope peaks at the value Ω_m, which satisfies Eq. (I.63) for the dispersion relation in Eq. (1), giving

$$\Omega_m = \left\{\frac{1}{2} + \frac{1}{2}\left[1 + 4\left(\frac{\omega_0 T}{3}\right)^2\right]^{1/2}\right\}^{1/2} \simeq 1 + \frac{1}{2}\left(\frac{\omega_0 T}{3}\right)^2, \tag{12}$$

where the last equality is valid for $\omega_0 T \ll 9/4$. One finds the peak value by inserting relation (12) into Eq. (11):

$$E_{\max} = \frac{|\beta|}{|z - i\beta|}\left(\frac{2c\omega_0}{\pi z}\right)^{1/2}(e\omega_0 T/3)^{-3/2}. \tag{13}$$

1. *On-Axis Temporal Width*

One may find the temporal width of the PB field in Eqs. (I.57) by solving

$$E(\Omega_d) = E_{\max}/d, \tag{14}$$

where d is a nondimensional attenuation factor. Solving this equation for any d is complicated. One may find a simple analytic solution by approximating the exponent in Eq. (11) by $\exp(-T\omega_0/2)$. The range of validity for this approximation is determined by the condition

$$\exp(-\omega_0 T\bar{\Omega}/2\sqrt{\bar{\Omega}^2 - 1}) > 0.9\exp(-\omega_0 T). \tag{15}$$

Solving inequality (15) with the condition $\omega_0 T \ll 9/4$ above yields

$$\bar{\Omega} > 1 + \frac{1}{2}\left(1 + \frac{1}{5\omega_0 T}\right)^{-2}. \tag{16}$$

Using this approximation in Eq. (14), we obtain

$$\Omega_d = \left[1 + d^{4/3}\left(\frac{\omega_0 Te}{3}\right)^2 \exp\left(-\frac{2}{3}T\omega_0\right)\right]^{1/2} \simeq 1 + \frac{1}{2}d^{4/3}\left(\frac{\omega_0 Te}{3}\right)^2 \exp\left(-\frac{2}{3}T\omega_0\right), \tag{17}$$

where the last equality is valid for

$$d \ll \left(\frac{\omega_0 Te}{3}\right)^{-3/2} \exp\left(\frac{1}{2}T\omega_0\right). \tag{18}$$

The temporal width Δ_t with respect to the wave front may be approximated via

$$\Delta_t \simeq \frac{z}{c}(\Omega_d - 1) = \frac{1}{2}\frac{z}{c}d^{4/3}\left(\frac{\omega_0 Te}{3}\right)^2 \exp\left(-\frac{2}{3}T\omega_0\right). \tag{19}$$

Comparing inequality (16) with relation (17), we find that the minimum value of d for which relation (19) is valid is given by

$$d > Q_d \equiv \left[\exp\left(-\frac{2}{3}T\omega_0\right)\left(\frac{\omega_0 Te}{3}\right)^2\left(1 + \frac{1}{5\omega_0 T}\right)^2\right]^{-3/4}, \tag{20}$$

where Q_d is the critical nondimensional parameter for the minimum attenuation d. Note that, in cases for which d does not satisfy the condition in inequality (18), Δ_t may be evaluated by the first equality in relation (19) with Ω_d evaluated by the first equality in relation (17).

The on-axis PB field obtained from Eqs. (I.57) (solid curve) for the dispersion relation in Eq. (1) as well as its envelope (dashed curve) in Eq. (11) are presented in Fig. 2. The PB parameters are $T = 0.005$ and $\beta/c = 5$, the dispersion parameter is $\omega_0 = 20\sqrt{2}$, and the field is evaluated at $z/c = 2$. Using relation (12), we find that the envelope peaks at $\Omega_m = 1.0011$, which corresponds to $t_m = \Omega_m z/c = 2.0022$. The peak value is found from Eq. (13), giving $E_{\max} = 60.73$ (note that here $\omega_0 T = 0.14 \ll 9/4$). Using these parameters, we find that the theoretical minimum value [Eq. (20)] for d is $Q_d = 5.4$ and that the temporal width in relation (19) corresponding to $d = 5.4$ is $\Delta_t = 0.1416$. This result is also shown in Fig. 2 by the thick line of length Δ_t, at the corresponding value of $E_{\max}/d$. This figure validates the result in relations (19) and (20).

2. *On-Axis Spatial Width*

Following the discussion in Subsection I.4.B.*2.b*, the on-axis envelope peaks at $z_m = ct/\Omega_m$, with Ω_m being given in relation (12) and its peak value being given by [cf. Eq. (13)]

$$E_{\max} = \frac{\beta}{\sqrt{{z_m}^2 + \beta^2}} \left(\frac{2c\omega_0}{\pi z_m}\right)^{1/2} (e\omega_0 T/3)^{-3/2}, \qquad z_m = \frac{ct}{\Omega_m}. \tag{21}$$

One may now find the on-axis spatial width of the field in Eqs. (I.57) by solving Eq. (14). Following the procedure given in relations (14)–(17), one finds that the on-axis spatial width Δ_z is

$$\Delta_z \simeq ct\left(1 - \frac{1}{\Omega_d}\right), \tag{22}$$

with Ω_d being given as in relation (17). The on-axis field (solid curve) for the same PB and dispersion parameters as in Fig. 2 but evaluated at $ct = 2$, as well as its envelope (dashed curve) in Eq. (11), are presented in Fig. 3. Using relation (12), we find that the envelope peaks at $\Omega_m = 1.0011$, which corresponds to $z_m = ct/\Omega_m = 1.9978$. The peak value $E_{\max} = 60.73$ is found from Eq. (13). As in Fig. 2, the theoretical minimum value [Eq. (20)] for d is $Q_d > 5.4$, and the on-axis width is $\Delta_z = 0.1322$ from relation (22). This result is also represented in Fig. 3 by the thick line of length Δ_z and at the corresponding value of $E_{\max}/d$. This figure validates the results given in relations (22) and (20).

3. *Off-Axis Spatial Width*

One obtains the off-axis spatial width of the PB field for the dispersion relation in Eq. (1) by inserting Eqs. (5) into Eq. (I.64). This yields

$$D(z, t) = \sqrt{\frac{I(z)c}{\omega_0}} (\bar{\Omega}^2 - 1)^{1/4}. \tag{23}$$

Results for three different observation times $t = 2.008$, 2.041, 2.096, which correspond to the first three (positive) peaks, respectively, of the on-axis field in Fig. 2, are presented in Fig. 4. The corresponding off-axis spatial widths in Eq. (23) are $2\sqrt{2}D = 0.3832$, 0.578, 0.717. These results are also represented in Fig. 4 by the thick lines of length $\sqrt{2}D$ and at the corresponding values of $E_{\max}/e$. Note that these values indeed quantify the off-axis widths of the field plots. The maximum off-axis deviation $\rho_{\max}$ for which the paraxial approximation in Eqs. (I.57) is valid is given in inequality (I.52). Using Eqs. (I.47) and (5) as well, one finds that, for the waveforms shown in Fig. 4, $\rho_{\max} = 1.90$, 1.93, 2.0 for Figs. 4(a), 4(b), and 4(c), respectively. These maximum off-axis deviations $\rho_{\max}$ are much greater than the corresponding off-axis spatial widths whence the D values above lie well within the legitimate range.

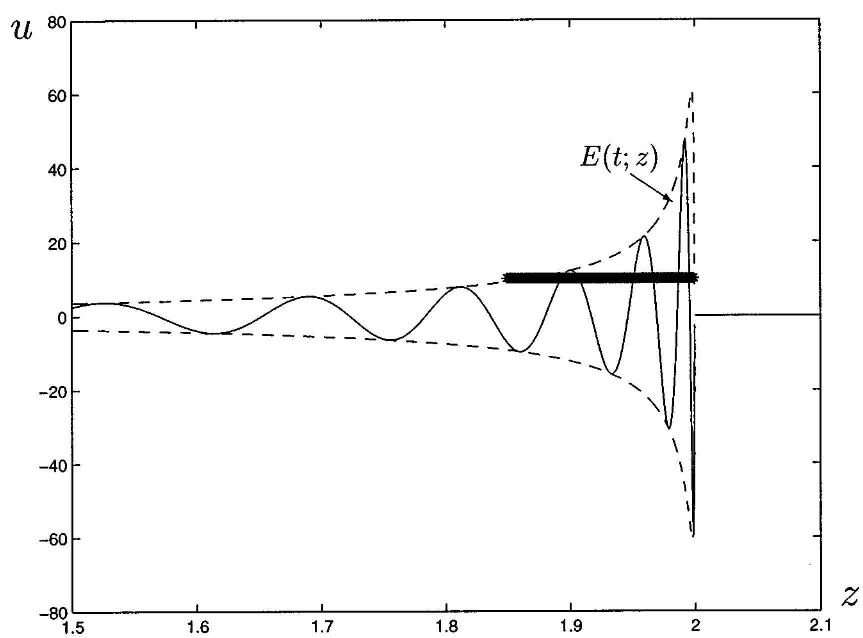

Fig. 3. Envelope function $E(t, z)$ (dashed curve) with constant t for the cold plasma dispersion. The thick line describes the approximated on-axis spatial width at $1/Q_d = 1/5.4$ of the envelope maximum. All quantities are normalized so that they bear dimensionality of length; i.e., $cT = 0.0005$, $\beta = 5$, $\omega_0/c = 20\sqrt{2}$.

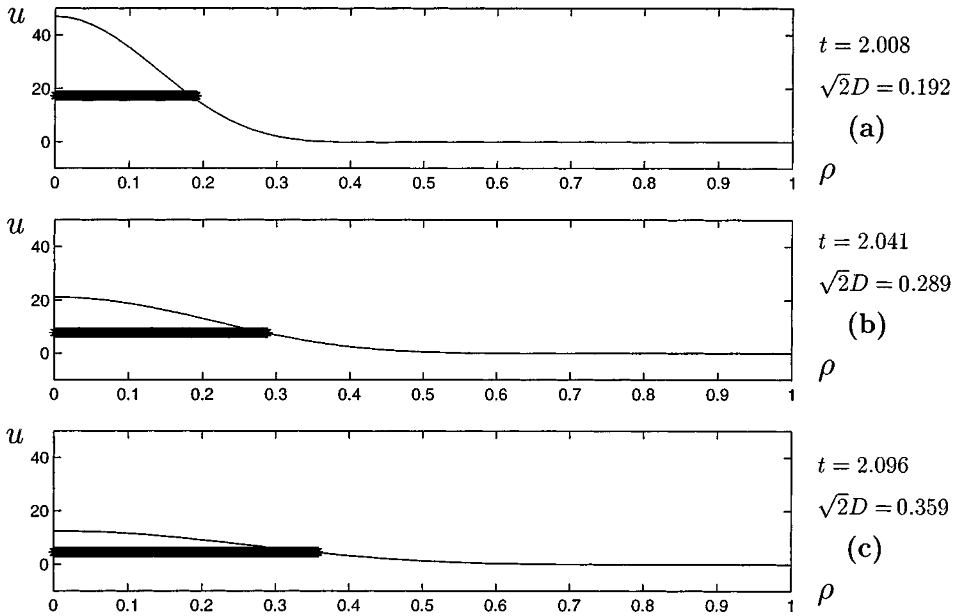

Fig. 4. Spatial (off-axis) width of the PB field for the cold plasma dispersion at various observation times.

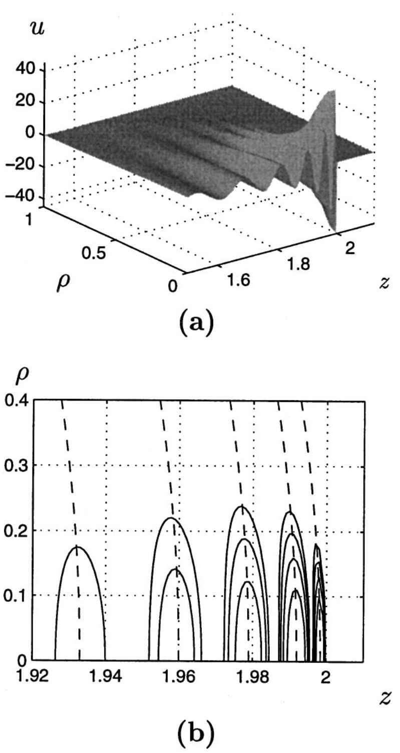

Fig. 5. PB field in the dispersive regime Eqs. (I.57) for the cold plasma dispersion relation with $\omega_0 = 20\sqrt{2}$. The field parameters are as in Fig. I.1). (a) PB in (ρ, z) plane, (b) contour plot of the field magnitude. The wave-front radii of curvature R_d [Eq. (I.70)] for various z values corresponding to the field maxima are also shown (dashed curves).

C. Wave-Front Radius of Curvature

As noted in Subsection I.4.B.*2.d*, the wave-front radius of curvature of the dispersive PB field is independent of the specific dispersion relation and is given by $R_d(z) = R(z) = (z - Z) + F^2/(z - Z)$ [Eq. (I.70)]. In Fig. 5(a) we present the dispersive PB field propagating in a cold plasma with dispersion relation (1) and $\omega_0 = 20\sqrt{2}$. The field parameters are as in Fig. I.1, i.e., $ct = 2$, $cT = 0.005$, and $\beta = 5$. The contour lines of the field magnitude as well as the radius of curvature $R_d(z)$ for several values of z (corresponding to local extrema) are presented in Fig. 5(b). Evidently these values of wave-front radii of curvature are in accord with the contour lines. These plots should be compared with the nondispersive pulse shape shown in Fig. I.1; the dispersive case exhibits prolonged oscillations.

D. Instantaneous Frequency

The instantaneous frequency $\omega_i(\mathbf{r}, t)$ for the generic dispersion relation $k(\omega)$ is given by [see Eq. (I.72)]

$$\omega_i(\mathbf{r}, t) = \bar{\omega}_s(z, t) - \frac{t}{z^2 k''(\bar{\omega}_s)} \frac{{}^1\!/_2\, \rho^2}{R(z)}. \tag{24}$$

We obtain the instantaneous frequency for the dispersion relation in Eq. (1) by inserting Eqs. (4) and (5) into Eq. (24), which gives

$$\omega_i(\mathbf{r}, t) = \frac{\omega_0 \bar{\Omega}}{\sqrt{\bar{\Omega}^2 - 1}} \left[1 + \frac{1}{2} \frac{\rho^2}{z} \frac{1}{R(z)(\bar{\Omega}^2 - 1)} \right]. \tag{25}$$

The term $(\omega_0 \bar{\Omega})/\sqrt{\bar{\Omega}^2 - 1}$ is the on-axis stationary frequency $\bar{\omega}_s(z, t)$ in Eq. (4); therefore the second term inside the bracket is the normalized deviation of the instantaneous frequency from $\bar{\omega}_s$. Under the paraxial approximation this deviation is proportional to ρ^2, and it is positive for $R(z) > 0$, i.e., for observers moving toward the waist location at Z [see Eq. (I.17)], but negative for observers moving away from Z. The result in Eq. (25) fails at observation points close to the wave front, where $\bar{\Omega} \to 1$ (see Section 3).

3. TRANSITION REGIME NEAR THE WAVE FRONT

A. Dispersion Surface

For observations near the wave front, where $\bar{\Omega} \to 1$ and the dispersion relation approaches the high-frequency limit $k(\omega) \to \omega/c$, the dispersive properties undergo a transition to the nondispersive regime, and the radius of curvature of the dispersion surface $\bar{R}_c \to \infty$. To parameterize the transition regime, we assume that the dispersion relation takes the form (Ref. 2, Section 1.6)

$$k(\omega) \sim \frac{\omega}{c} - \frac{{\omega_\alpha}^2}{c\,\omega}, \qquad \omega \to \infty \tag{26a}$$

with ω_α denoting a characteristic frequency parameter. Dispersion relations as in relation (26a) are characteristic of lossless Lorentz-type materials.[3] We then find the stationary frequency $\bar{\omega}_s$ by using relation (26a) in Eqs. (I.45), obtaining

$$\bar{\omega}_s = \omega_\alpha / \sqrt{\bar{\Omega} - 1}. \tag{26b}$$

Since $\bar{\omega}_s \to \infty$ as the observation point approaches the wave front $\bar{\Omega} \to 1$, the asymptotic evaluation via the isolated saddle point, which leads to Eqs. (I.57), becomes invalid. The corresponding transitional radius of curvature of the dispersion surface is obtained through relations (I.47) and (26a) by

$$\bar{R}_c = \frac{-\omega_\alpha}{2}\left(\frac{\bar{\Omega}^2 + 1}{\bar{\Omega} - 1}\right)^{3/2}. \tag{27}$$

From relations (27) and (I.52) we can assess the transitional behavior of the paraxial PB wave packet, which now satisfies the condition in relation (I.52) with

$$\rho_{\max} = \left[\frac{32\pi c z |z - i\beta|^2}{\omega_\alpha}\,\frac{(\bar{\Omega} - 1)^{3/2}}{\bar{\Omega}^2}\right]^{1/4}. \tag{28}$$

Clearly, the paraxial off-axis range shrinks as $\bar{\Omega} \to 1$ and is influenced as before by the beam parameters as well as by the dispersion parameter ω_α.

B. Transitional Beam Fields

As noted above, the transitional beam field near the wave front $z = ct$ can no longer be described by the simple saddle-point evaluation formula. To derive the transition function we assume that

$$\hat{f}(\omega) \sim \exp[-(1/2)T\omega], \qquad \omega \to \infty, \tag{29}$$

where T parameterizes the maximum frequency of $\hat{f}$ through relation (I.21); this behavior is in accord with the analytic wave packet in Eqs. (I.20a). For plane-wave inputs the $k(\omega)$ dependence in relation (26a) permits a closed-form inversion of the integral in Eq. (I.18) (see Ref. 2). We shall seek a similar closed-form result for the beam input in Eq. (I.8), with relation (29).

To stabilize the resulting inversion integral [Eq. (I.18)] [see discussion in relation to Eq. (31)], we include in relation (29) a low-frequency convergence factor

$$\hat{f}(\omega) \sim \exp[-(1/2\,T\omega + a/\omega)], \qquad \omega \to \infty, \qquad a > 0, \tag{30}$$

which does not affect the $\omega \to \infty$ limit in relation (29). In particular, for $\omega \gg \sqrt{a/T}$, relation (30) reduces to relation (29). To recover the time-domain field $u(\mathbf{r}, t) = \operatorname{Re} \overset{+}{u}(\mathbf{r}, t)$ from the analytic signal representation, we insert relations (26a) and (30) into Eq. (I.18) to obtain

$$\overset{+}{u}(\mathbf{r}, t) = \frac{1}{\pi}\frac{-i\beta}{z - i\beta}\int_0^\infty \mathrm{d}\omega \exp[-i\omega\tau - i\bar{b}(1/\omega)],$$

$$\tau = t - i\frac{T}{2} - \frac{S}{c}, \qquad \bar{b} = \frac{{\omega_\alpha}^2 S(\mathbf{r})}{c} - ia. \tag{31}$$

Note that, to ensure convergence as $\omega \to 0$, we must have $\operatorname{Im}\bar{b} \leqslant 0$. Therefore, for a given $\mathbf{r}$, where $\operatorname{Im} S \geqslant 0$, a should be chosen such that $\operatorname{Im} S \leqslant ca/{\omega_\alpha}^2$. Using Eq. (I.14), we obtain

$$a \geqslant \frac{1}{2}\rho^2\frac{{\omega_\alpha}^2}{c}\left\{\beta_r\left[1 + \left(\frac{z + \beta_i}{\beta_r}\right)^2\right]\right\}^{-1}. \tag{32}$$

The integral in Eq. (31) may be evaluated in closed form in terms of a Hankel function with complex argument (Ref. 4, Section 3.6.5):

$$\overset{+}{u}(\mathbf{r}, t) = \frac{i\beta}{z - i\beta}\sqrt{\frac{\bar{b}}{\tau}}\,H_1^{(2)}(2\sqrt{\bar{b}\tau}), \tag{33a}$$

$$\overset{+}{u}(\mathbf{r}, t) \sim \frac{i\beta}{z - i\beta}\sqrt{\frac{b}{\tau}}\,H_1^{(2)}(2\sqrt{b\tau}), \qquad b = \frac{{\omega_\alpha}^2 S}{c}. \tag{33b}$$

The locally uniform result in Eq. (33a) parameterizes the time-domain response in the near-wave-front regime of high frequencies where relation (26a) applies, either at the wave front where $\bar{b}\tau \to 0$ or far enough behind the wave front so that $\bar{b}\tau \gg 1$, but within the near-wave-front regime $\bar{\Omega} = ct/z \simeq 1$. Since the large-$\omega$ contribution is not affected by the a/ω term in relation (30), we can set $a = 0$, thereby replacing $\bar{b}$ by b to obtain relation (33b).

C. Transitional On-Axis Response

For on-axis points, where $\rho = 0$, the PB propagator behaves like a one-dimensional plane wave. To compare the above result with the plane-wave result given in Ref. 2, we assume that $T = 0$ (impulsive response), obtaining $S = z$, $b = {\omega_\alpha}^2 z/c$. Since the argument $\sqrt{b\tau}$ is now real, the real and the imaginary parts of the Hankel function are given by J_1 and $-Y_1$, respectively. In the plane-wave limit the collimation length $F = \beta_r \gg z$ [see Eqs. (I.15)], so we may approximate $(-i\beta)/(z - i\beta) \simeq 1$. Thus, by taking the real part of relation (33b), we obtain

$$u(z, t) = -\sqrt{b/\tau}\,J_1(2\sqrt{b\tau}), \tag{34}$$

which is an expression exactly the same as the one found in Ref. 2, Eq. 1.7.49, with $\nu = 0$.

D. Very near the Wave Front: Nondispersive Limit

To obtain a simple expression for the field very near the wave front, we assume that $|2\sqrt{b\tau}| \ll 1$, that is,

$$|2\sqrt{b\tau}| = 2\left|t - i\,\frac{T}{2} - \frac{S}{c}\right|^{1/2}\left|\frac{\omega_\alpha{}^2 S}{c}\right|^{1/2} \ll 1. \tag{35}$$

In this case we may use the small argument approximation for the Hankel function, $H_1^{(2)}(z \ll 1) \sim -2(\pi i z)^{-1}$, reducing relation (33b) to

$$\begin{aligned}\overset{+}{u}(\mathbf{r},\,t) &= \frac{-i\beta}{z - i\beta}\,\frac{1}{\pi i}\,\frac{1}{\tau}\\ &= \frac{-i\beta}{z - i\beta}\,\overset{+}{\delta}\Big\{t - i\,\frac{T}{2}\\ &\qquad - c^{-1}\Big[z + \frac{1}{2}\,\rho^2/(z - i\beta)\Big]\Big\}.\end{aligned} \tag{36}$$

This expression is exactly the same as the nondispersive wave packet in Eq. (I.22) and therefore demonstrates the range of validity of the isodiffracting initial conditions: The field very near the wave front is a wave packet, well localized in space–time. The parameterization of this wave packet was discussed in Subsection I.4.A.

The approximation in Eq. (36) is valid for space–time points that satisfy inequality (35). For on-axis observation point $z = ct$, inequality (35) takes the form

$$Q_\Omega \equiv 2\left\{\frac{\omega_\alpha{}^2 z}{c}\left[\left(t - \frac{z}{c}\right)^2 + \left(\frac{T}{2}\right)^2\right]^{1/2}\right\}^{1/2} \ll 1. \tag{37}$$

Using the parameter $\bar{\Omega} = ct/z$ in inequality (37), we obtain

$$Q_\Omega \equiv 2\,\frac{\omega_\alpha z}{c}\left[(\bar{\Omega} - 1)^2 + (\bar{\Omega}_T/2)^2\right]^{1/4} \ll 1, \tag{38}$$

where $\bar{\Omega}_T = cT/z$. Q_Ω is the nondimensional critical parameter that parameterizes the maximum distance $\Omega_{\lim}$ behind the wave front for which the field remains localized and may be regarded as a nondispersive wave packet. With inequality (38), $\bar{\Omega}_{\lim}$ is given explicitly by

$$\bar{\Omega}_{\lim} = 1 + \left[\left(\frac{c}{2z\omega_\alpha}\right)^4 - (\bar{\Omega}_T/2)^2\right]^{1/2}. \tag{39}$$

For $\bar{\Omega} \gg \bar{\Omega}_{\lim}$, the field is subject to dispersion as discussed in Subsection 3.E.

At the wave-front on-axis observation point $z = ct$, $\rho = 0$, and $\bar{\Omega} = 1$, Eq. (39) takes the form

$$Q_\gamma \equiv Q_\Omega|_{\Omega=1} = \omega_\alpha\sqrt{\frac{2Tz}{c}} \ll 1. \tag{40}$$

By choosing the dimensionless parameter Q_γ according to inequality (40) we ensure that all the nondispersive beam parameterizations in Eqs. (I.22) and (I.23) remain valid in the limit very near the wave front. Recalling relation (I.21), we may interpret inequality (40) in the following manner: For a given z, the maximum excitation frequency required for the field to remain localized is given by $\omega_{\max} \gg 2z\omega_\alpha{}^2/c$.

E. Behind the Wave Front: Dispersive Limit

For $2\sqrt{b\tau} \gg 1$, we may use the large argument approximation for the Hankel function, $H_1^{(2)}(z) \sim \sqrt{2/\pi z}\,\exp(-iz + 3/4\pi i)$. Thus the field sufficiently far behind the wave front (but still in the near-wave-front range) is given by

$$\overset{+}{u}(\mathbf{r},\,t) \sim -\frac{-i\beta}{z - i\beta}\,\sqrt{\frac{b}{\tau}}\sqrt{\frac{1}{\pi\sqrt{b\tau}}}\,\exp(-i2\sqrt{b\tau} + {}^3\!/_4\,\pi i). \tag{41}$$

To compare this result with the asymptotic field in Eqs. (I.57), we derive, from relations (I.54), (26a), and (31),

$$\begin{aligned}\omega_s \equiv \omega_s(\mathbf{r},\,t) &= \omega_\alpha\left[\frac{c(t - iT/2)}{S} - 1\right]^{-1/2}\\ &= \sqrt{\frac{b}{\tau}}\,,\end{aligned}$$

$$2\sqrt{b\tau} = (t - iT/2)\omega_s(\mathbf{r},\,t) - k(\omega_s)S, \tag{42}$$

and finally

$$k''(\omega_s) = \frac{-2\omega_\alpha{}^2}{c}\,\omega_s{}^{-3} = \frac{-2\omega_\alpha{}^2}{c}\left(\frac{b}{\tau}\right)^{-3/2}. \tag{43}$$

Using Eqs. (42) and (43) in relation (41), we obtain

$$\begin{aligned}\overset{+}{u}(\mathbf{r},\,t) &\sim \frac{-i\beta}{z - i\beta}\,\frac{1}{\pi}\left[\frac{-2\pi}{ik''(\omega_s)S}\right]^{1/2}\exp(-i\Psi),\\ \Psi &= (t - iT/2)\omega_s(\mathbf{r},\,t) + ik(\omega_s)S,\end{aligned} \tag{44}$$

which is the complete asymptotic expression for the integral in Eq. (I.18). We obtain the paraxial approximation in Eqs. (I.57) by expanding the phase in relations (44) up to second order in ρ and up to first order in T and the amplitude up to zero order about $\rho = 0$, $T = 0$ [recall from Eqs. (I.54) and (I.26) that $\omega_s|_{\rho=0,T=0} = \bar{\omega}_s$]. Also note that the conditions in inequalities (I.52) and (I.59) correspond to neglecting the next-order nonzero terms $\partial^4\Psi/\partial\rho^4$ and $\partial^2\Psi/\partial T^2$, respectively. Thus the dispersive limit for the approximate dispersion relation in relation (26a) blends smoothly with the full generic dispersion expressed by $k(\omega)$ in the common domain within the near-wave-front range in which both are valid simultaneously.

The bilateral matching parameterized by Q_γ in inequality (40) is presented in Fig. 6 for the dispersion relation in relation (26a). The figure describes the on-axis PB field with $T = 0.005$, $\beta/c = 5$ at $z/c = 2$. The dispersion parameter is $\omega_\alpha = 0.2, 5, 20$, which corresponds to $Q_\gamma = 0.071, 0.71, 2.8$ [see inequality (40)]. These values of Q_γ parameterize the PB field in the nondispersive, transition, and dispersive regimes for Figs. 6(a), 6(b), and 6(c), respectively. The field is evaluated in three different forms: by the near-wave-front uniform solution evaluated with the analytic Hankel function in relation (33b), by the nondispersive solution in Eq. (36), and by the dispersive asymptotic solution in relation (41). In Fig. 6(a) the uniform solution and the nondispersive field are almost identical, inasmuch as here $Q_\gamma = 0.071 \ll 1$; the field is also evaluated by a direct fast-Fourier-transform integration of Eq. (I.18) to calibrate the analytic solution (both solutions coincide in the figure). By contrast, the asymptotic solution does not reconstruct the field. Figure 6(b) describes the field in the transition regime with $Q_\gamma = 0.71$. Here neither the nondispersive solution nor the asymptotic solution agrees with the uni-

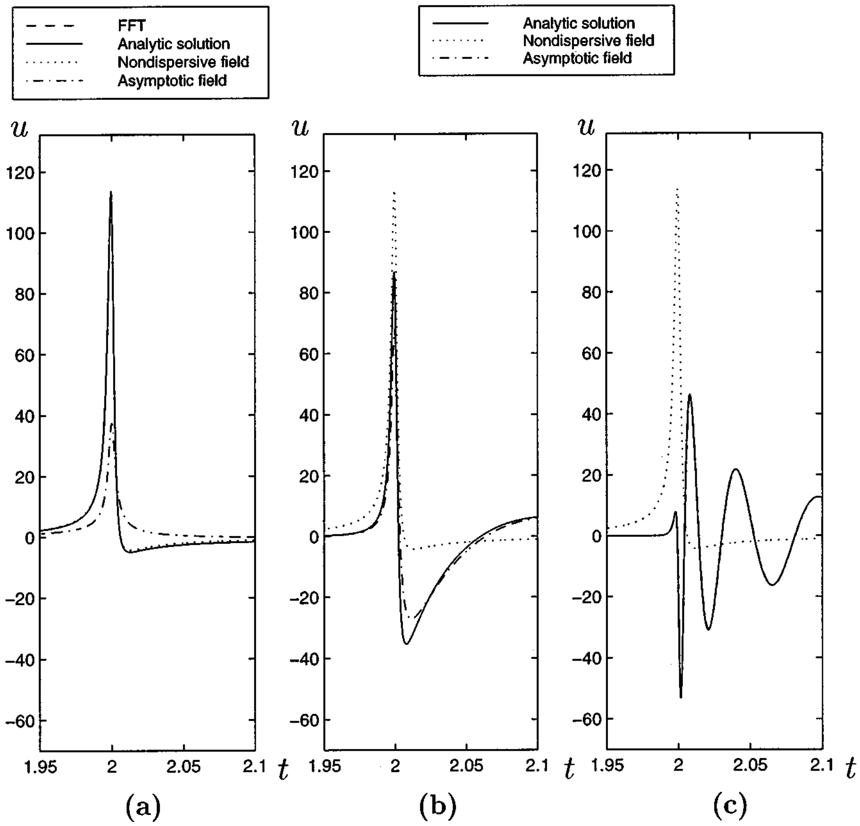

Fig. 6. Bilateral matching for the on-axis PB field of relation (33b) in the medium of relation (26a): $z/c = 2$; $T = 0.005$; $\beta/c = 5$, with $Q_\gamma = 0.071, 0.71, 2.8$ for (a), (b), and (c), respectively.

form field. Finally, Fig. 6(c) describes the field in the dispersive regime ($Q_\gamma = 2.8 > 1$) in which the uniform and the asymptotic solutions coincide.

4. CONCLUSION

In this second part of a two-part investigation we have extended the theory of pulsed-beam propagation in homogeneous lossless dispersive media from the full dispersive regime addressed in Part I[1] to the dispersive-to-nondispersive transition regime near the wave front. We have also performed numerical experiments for a simple Lorentz-type dispersion model to assess the accuracy of the various asymptotic field representations, estimators, and nondimensional critical parameters that quantify the effects of dispersion on the pulsed-beam physical observables. The results confirm that the estimates on domains of validity work, and the critical parameters are indeed matched to the problem. While the simple test so far is not conclusive, it does suggest that the procedures employed are on the right track.

Further studies will deal with the inclusion of dissipation in the $k(\omega)$ model and with nonhomogeneous medium profiles.

ACKNOWLEDGMENTS

This research was supported in part by the Naval Coastal Systems Center, Panama City, Florida, under Office of Naval Research grant N61331-96-K-0028. Also, T. Melamed acknowledges partial support from a 1996-97 Dean's Postdoctoral Fellowship at Boston University, and L. B. Felsen acknowledges partial sponsorship under U.S.–Israel Binational Science Foundation grant 95-00399.

*Also with the Department of Electrical and Computer Engineering, Boston University, Boston, Massachusetts 02215.

REFERENCES

1. T. Melamed and L. B. Felsen, "Pulsed-beam propagation in lossless dispersive media. I. Theory," J. Opt. Soc. Am. A **15**, 1268–1276 (1998).
2. L. B. Felsen and N. Marcuvitz, *Radiation and Scattering of Waves* (IEEE, Piscataway, N.J., 1994). Classic reissue.
3. K. E. Oughstun and G. C. Sherman, *Electromagnetic Pulse Propagation in Causal Dielectrics*, Vol. 16 of Springer Series on Wave Phenomena (Springer, New York, 1997).
4. W. Magnus, F. Oberhettinger, and R. P. Soni, *Formulas and Theorems for the Special Functions of Mathematical Physics* (Springer-Verlag, New York, 1966).